universe

MDPI

Article

Characterizing Timing Noise in Normal Pulsars with the Nanshan Radio Telescope

Jianping Yuan [1,2,*], Na Wang [1], Shijun Dang [3], Lin Li [4], Feifei Kou [1], Wenming Yan [1], Zhigang Wen [1], Zhiyong Liu [1], Rai Yuen [1], Jingbo Wang [5], Zurong Zhou [6], Peng Liu [7] and Dalin He [1]

1 Xinjiang Astronomical Observatory, Chinese Academy of Sciences, 150 Science 1-Street, Urumqi 830011, China; na.wang@xao.ac.cn (N.W.); koufeifei@xao.ac.cn (F.K.); yanwm@xao.ac.cn (W.Y.); wenzhigang@xao.ac.cn (Z.W.); liuzhy@xao.ac.cn (Z.L.); ryuen@xao.ac.cn (R.Y.); hedalin@xao.ac.cn (D.H.)
2 Key Laboratory of Radio Astronomy, Chinese Academy of Sciences, Urumqi 830011, China
3 School of Physics and Electronic Science, Guizhou Normal University, Guiyang 550001, China; dangsj@gznu.edu.cn
4 School of Physical Science and Technology, Xinjiang University, Urumqi 830017, China; lilin@xao.ac.cn
5 Institute of Optoelectronic Technology, Lishui University, Lishui 323000, China; 1983wangjingbo@163.com
6 National Time Service Center, Chinese Academy of Sciences, Xi'an 710600, China; zhouzurong@ntsc.ac.cn
7 Department of Astronomy, Xiamen University, Xiamen 361005, China; 34820210156871@stu.xmu.edu.cn
* Correspondence: yuanjp@xao.ac.cn

Abstract: We present a decade of observations of pulse arrival times for 85 pulsars using the Nanshan radio telescope from July 2002 to March 2014. The Cholesky method can accurately estimate the covariance function of the timing residuals, significantly improving the parameter's estimation accuracy when red noise is prominent. We utilize the Cholesky method to determine positions and basic timing parameters of these pulsars, as well as to obtain timing residuals. Most of these sources showed evidence of significant timing irregularities, which are described. The spectral analyses of timing residuals are presented for pulsars showing obvious red noise. Our results show that timing residuals in half of these pulsars are attributed to rotational irregularities. The red noise in normal pulsars may originate from a random walk in spin frequency or spin-down rate.

Keywords: neutron star; radio pulsar; timing noise

Citation: Yuan, J.; Wang, N.; Dang, S.; Li, L.; Kou, F.; Yan, W.; Wen, Z.; Liu, Z.; Yuen, R.; Wang, J.; et al. Characterizing Timing Noise in Normal Pulsars with the Nanshan Radio Telescope. *Universe* **2024**, *10*, 105. https://doi.org/10.3390/universe10030105

Academic Editor: Nicolas Chamel

Received: 30 December 2023
Revised: 19 February 2024
Accepted: 21 February 2024
Published: 26 February 2024

1. Introduction

The regular increase in spin period detected in most pulsars is associated with the kinetic energy loss from the rotating neutron star. Nevertheless, timing observations have shown that the rotations of many pulsars are affected by two types of irregularities: glitches and timing noise [1,2]. Pulsar glitches reveal a sudden increase in the rotation rate, providing physical information and constraining models for the internal and crustal dynamics [3]. The timing noise of the pulsar was first detected through timing observations of the Crab pulsar [4]. After fitting the spin-down model, the timing residuals exhibited a quasi-sinusoidal structure, which was suggested to be caused by rotational irregularities. It was proposed that the rotation of a pulsar was affected by a random walk in the pulse phase, spin frequency (or angular velocity), and spin-down rate (or torque) [4]. These processes were referred to as phase noise (PN), spin noise (FN), and spin-down noise (SN), respectively. The statistical properties of the Crab pulsar suggested that it follows a random walk in spin frequency [5–7]. However, further studies cast doubt on it. The timing noise of 24 pulsars was examined, and the conclusion was that the timing irregularities observed in many pulsars could not be simply modeled as a random walk process [8]. The 14.5 yr timing behavior of the Vela pulsar demonstrated that most of its noise properties arise from individual discontinuities in spin frequency and frequency derivative, rather than random fluctuations [9]. The timing irregularities of 366 pulsars were studied, leading

to the conclusion that the timing residuals could not simply be modeled as a random walk [2,8].

To quantify the irregularity of a pulsar's rotation, a parameter defined as $\Delta_8 = \log(\ddot{\nu}t^3/(6\nu))$ was introduced, where ν and $\ddot{\nu}$ are measured over a duration of 10^8 s ($\sim$3.16 yr) [10]. The relationship between Δ_8 and the period derivative was investigated [2]. It turned out that there is a correlation between timing noise and spin-down rate: pulsars with higher spin-down rates exhibit more significant timing noise [11]. A statistic based on Allen variance, $\sigma_z = \langle c^2 \rangle^{1/2} \tau^2 / \left(2\sqrt{5}\right)$, can be used to measure irregularities on various time scales [12]. Bayesian software TempoNest (version 1.0) and ENTERPRISE (version 3.0) were developed and used to characterize the timing parameters and power spectra of normal pulsars and millisecond pulsars [13–16].

Spectral analysis of the residual pulse arrival times of pulsars can provide valuable insights into the theoretical models that account for the timing noise [17]. Applying the standard Fourier method, researchers found that the timing residuals of the Crab pulsar showed a power spectrum that closely resembled a frequency jump noise model [4]. Based on the orthonormal polynomials, a new technique was developed to minimize the impact of uneven sampling and non-uniform data quality [5,6]. This method provides a low-resolution but reasonable estimation of power spectra for the timing data across various frequencies. This study demonstrated that the timing noise observed in the Crab pulsar was consistent with a random walk in the rotation frequency. A similar technique was used to analyze the timing noise of 11 pulsars. The results suggested that they show a random walk in rotational phase, frequency or frequency derivative [18]. The orthonormal polynomials were used as power spectral density estimators to minimize the leakage of low-frequency and high-frequency power [19,20]. Four pulsars were investigated with the power spectral density of the timing residuals [21]. The cubic term arises from the red torque noise in the random walk of pulse frequency derivatives, which may result from external torques exerted by the magnetosphere of the pulsar. The CLEAN technique was introduced and applied to derive the power spectra of timing noise observed in 18 southern pulsars [22,23]. The results indicated that the majority of the spectra can be accurately described by a single- or double-component power law model. A pre-whitening method was proposed for spectral estimation to eliminate spectral leakage and provide nearly independent spectral estimates [24].

In this paper, we report on nearly a decade of observations of pulse arrival times for a group of pulsars using the Nanshan 25 m radio telescope, which was upgraded to 26 m in 2015. Timing residuals were obtained for a total of 85 isolated pulsars, and 55 of these exhibited significant timing irregularities. Basic timing parameters are determined for these pulsars, and the observed timing irregularities are described. The spectral analyses are presented for the noisy pulsars showing significant red noise.

2. Observations and Data Analysis

The Nanshan pulsar timing project was launched in January of 2000 with the 25 m radio telescope and a room temperature receiver [25]. Each observation was performed with a center frequency of 1540 MHz with a total bandwidth of 320 MHz. A cryogenic receiver was put into operation in 2002 July with a system temperature of ~20 K [26]. The down-converted signals from the polarization channels of the linear feeds were fed into an analog back end. The back end produces a filter bank output comprising 128 frequency channels with 1-millisecond sampling. The signals were 1-bit digitized and folded at the topocentric pulse period obtained from the pulsar catalogue (PSRCAT) [27]. Data were accumulated for 60 s with 256 phase bins across the pulse period and then written in the timer format to disk. The timestamp was synchronized with the station clock, which is derived from a hydrogen maser and was referenced to Coordinated Universal Time via the Global Positioning System network. A digital filter bank (DFB) has been used since 2010. The device converts analog voltages into digital signals, which are then processed using a polyphase filter in field-programmable gate array processors. The correlators in the pulsar processing unit (PPU) then generate the polarization products, fold every 30 s signals at the

known pulse period, then save in the PSRFITS format to a disk. Each pulsar is typically observed on three epochs every month with an exposure time of four to sixteen minutes. The timing data extend from July 2002 to March 2014. Except for the datasets from PSRs J1041−1942 and J2321+6024, which are obtained with both the room temperature receiver and the cryogenic receiver, the data for other 83 pulsars are acquired with the latter. As the Nanshan radio telescope underwent a comprehensive upgrade, leading to a two-year gap in the dataset, we will leave the dataset since 2016 for future research.

Offline analyses are conducted using the PSRCHIVE package [28]. After mitigating the radio frequency interference (RFI) in the data, each observation was incoherently dedispersed, scrunched in time, frequency, and polarization to create a total intensity integrated pulse profile. In order to obtain the pulse TOA, each of the total intensity profiles was cross-correlated with a high signal-to-noise ratio "standard template", and this template was obtained by summing all available data for each system. Timing residuals were calculated after transforming the TOA to the solar system barycenter using the pulsar timing software package TEMPO2 (version 2022.05.01) [29,30] with the Jet Propulsion Laboratory's (JPL) planetary ephemeris DE414 [31]. The observatory clock offsets are corrected to refer the ToAs to International Atomic Time (TAI) using TEMPO2. Each observed TOA was initially referenced to terrestrial time (BIPM2015) and then to Barycentric Coordinate Time (TCB). For each pulsar, the timing analysis package TEMPO2 was used to determine a phase-connected timing solution that includes the pulse frequency ν and its first derivative $\dot{\nu}$. This package employs least-squares fitting of the spin-down model to the TOA data. The dispersion measures are fixed in the fitting. TOA errors are often underestimated due to potential temporal variations in the pulse shape, lingering radio frequency interference (RFI), or imperfect templates. Therefore, an uncertainty factor (EFAC) is included as a multiplicative correction for the measured TOA uncertainties. The spin-down model can be expressed using Taylor series as:

$$\Phi(\mathrm{t}) = \Phi_0 + \nu(t - t_0) + \frac{1}{2}\dot{\nu}(t - t_0)^2 + \frac{1}{6}\ddot{\nu}\,(t - t_0)^3 \quad (1)$$

where Φ_0 is the pulse phase at the time t_0; ν, $\dot{\nu}$, and $\ddot{\nu}$ are the rotation frequency, its first derivative, and its second derivative.

The power spectra of timing residuals are estimated using the Cholesky method and employing the spectralModel plugin in the TEMPO2 package. First, we generate timing residuals using the initial models of the pulsars, and apply a linear transformation (based on the Cholesky decomposition) of the covariance matrix of the timing residuals, to pre-whiten the residuals. The spectralModel plugin for TEMPO2 is used to estimate analytical models for the spectra of the red noise components of the timing residuals. Then, the red noise can be parameterized by fitting a power law model as follows: $P(f) = A/[1 + (f/f_c)^2]^{\alpha/2}$, where A is the spectral amplitude, f_c represents the corner frequency (at which the power law component reaches the white noise level), and α is the spectral index [24]. With the analytic red noise model, we fit the pulsar parameters, including the positions and spin parameters, using the global least squares fitting procedure. This allow us to obtain the final improved parameters and uncertainties [24]. We include the second derivative of spin frequency in the timing model only when the estimated value exceeds 3σ of the uncertainty. The parameters for the power spectra of red noise are determined, but the uncertainties in the noise parameters are not provided by the spectralModel plugin. Based on our experience with this plugin, we estimate that there would be uncertainty in the spectral index of ~0.2.

3. Results

In this section, we present the results of our timing analyses of 85 pulsars. Compared with the uncertainties in TOAs, the error in the solar system ephemeris could be negligible, although it is possible that it could mimic timing noise. Assuming that the dispersion measure (DM) noise is also negligible, we did not fit DM in our analysis. Although

glitches were reported to occur in five pulsars (PSRs J0215+6218, J0502+4654, J0601−0527, J0855−3331, and J2225+6535), we include these pulsars in this paper, as these events have small magnitudes with $\Delta\nu/\nu < 6 \times 10^{-9}$ between MJD 52,616 and 55,965. For instance, two small glitches in J2225+6534 were detected with $\Delta\nu/\nu = 0.30(1) \times 10^{-9}$ and $\Delta\nu/\nu = 1.65(2) \times 10^{-9}$ using the Nanshan radio telescope [32]. The ephemerides of 85 sources were initially obtained from PSRCAT [27], and updated positions and rotational parameters (such as spin frequency, spin frequency first derivative, and second derivative) were calculated using TEMPO2 and the Cholesky method. The epochs of the timing model were set to an integral Modified Julian Date (MJD) near the center of the data span. The derived parameters are presented in Table 1. The pulsars' J2000 name, epoch, right ascension, and declination in J2000 coordinates are listed in columns 1, 2, 3 and 4. The following three columns provide information on the rotational frequency, frequency derivative, and frequency second derivative. The uncertainties, given in parentheses after each quantity as the error in the least significant digit, represent the standard errors obtained from TEMPO2.

Table 1. Positions in J2000 equatorial coordinates and rotational parameters of 85 pulsars.

PSR Name	Epoch	RAJ (h:m:s)	DECJ (d:m:s)	ν (Hz)	$\dot{\nu}$ ($\times 10^{-15}$ s^{-2})	$\ddot{\nu}$ ($\times 10^{-25}$ s^{-2})
J0040+5716	54,596	00:40:32.379(4) *	+57:16:24.83(3)	0.8942731376217(8)	−2.302373(8)	0.007(2)
J0102+6537	54,593	01:02:32.958(16)	+65:37:13.40(11)	0.595533454184(2)	−2.12071(2)	0.120(6)
J0108+6608	54,548	01:08:22.64(5)	+66:08:34.0(3)	0.77901947917(7)	−7.8571(6)	−12.2(2)
J0147+5922	54,532	01:47:44.647(2)	+59:22:03.286(21)	5.093688465822(2)	−6.65973(2)	0.070(5
J0152−1637	54,611	01:52:10.855(3)	−16:37:53.44(6)	1.200851630721(1)	−1.87472(1)	−0.017(3)
J0215+6218	54,610	02:15:56.626(10)	+62:18:33.37(10)	1.8218918032386(12)	−2.200750(13)	0.103(4)
J0323+3944	54,804	03:23:26.65(3)	+39:44:52.3(8)	0.329074382841(13)	−0.06912(2)	-
J0357+5236	54,594	03:57:44.830(2)	+52:36:57.57(4)	5.075361662901(3)	−12.28359(3)	−0.671(8)
J0448−2749	54,596	04:48:41.567(6)	−27:49:46.74(11)	2.220010185046(6)	−0.73288(5)	−0.095(15)
J0502+4654	54,586	05:02:04.559(3)	+46:54:06.40(8)	1.5660031444061(14)	−13.691955(12)	−0.199(4)
J0601−0527	54,595	06:01:58.979(1)	−05:27:50.78(3)	2.525445361737O(13)	−8.306389(13)	0.040(4)
J0624−0424	54,584	06:24:20.028(3)	−04:24:50.45(11)	0.9623927426388(7)	−0.769143(14)	-
J0659+1414	54,593	06:59:48.177(21)	+14:14:21.8(17)	2.597980592784(5)	−370.98321(4)	5.830(14)
J0729−1836	54,593	07:29:32.346(7)	−18:36:42.20(14)	1.960137336447(18)	−72.87551(17)	1.44(5)
J0758−1528	54,594	07:58:29.0635(12)	−15:28:08.53(3)	1.46570432666699(9)	−3.483819(9)	0.131(3)
J0855−3331	54,455	08:55:38.413(7)	−33:31:39.30(11)	0.7889308472924(21)	−3.93390(4)	-
J0943+1631	54,590	09:43:30.11(5)	+16:31:36.4(21)	0.919609748204(3)	−0.07674(3)	0.014(8)
J1041−1942	54,130	10:41:36.197(3)	−19:42:13.43(7)	0.72130892604934(4)	−0.491612(7)	-
J1115+5030	54,593	11:15:38.427(6)	+50:30:11.46(7)	0.6037039950853(4)	−0.908551(7)	-
J1257−1027	54,592	12:57:04.769(16)	−10:27:05.8(6)	1.619937323186(2)	−0.95087(2)	0.023(7)
J1320−3512	54,514	13:20:12.599(4)	−35:12:27.02(7)	2.1810801949582(15)	−0.00311(3)	-
J1532+2745	54,585	15:32:10.364(9)	+27:45:49.4(14)	0.8890184155611(13)	−0.616216(28)	-
J1543+0929	54,596	15:43:38.82(4)	+09:29:16(1)	1.336097009317(7)	−0.77053(6)	0.115(18)
J1555−3134	54,595	15:55:17.951(3)	−31:34:20.25(11)	1.9300927611908(7)	−0.231743(14)	-
J1603−2712	54,595	16:03:08.063(9)	−27:13:27.6(6)	1.284827790027(4)	−4.96856(4)	0.104(11)
J1623−0908	54,545	16:23:17.654(8)	−09:08:49.4(5)	0.783424529909(1)	−1.58391(2)	-
J1701−3726	54,480	17:01:18.48(2)	−37:26:26.4(8)	0.407395851005(2)	−1.846776(19)	0.031(6)
J1711−1509	54,594	17:11:55.059(9)	−15:09:39.7(7)	1.1510066530733(3)	−1.45899(3)	0.088(8)
J1720−1633	54,382	17:20:25.206(11)	−16:33:33.7(15)	0.638731315014(3)	−2.37246(3)	−0.018(10)
J1722−3712	54,606	17:22:59.184(11)	−37:12:07.5(5)	4.234076085331(6)	−194.635(3)	5.7(9)
J1733−3716	54,598	17:33:26.763(4)	−37:16:55.12(18)	2.962138716670(7)	−132.00573(7)	−0.446(21)
J1738−3211	54,525	17:38:54.185(9)	−32:11:53.6(6)	1.3012373664386(22)	−1.34575(2)	0.029(7)
J1739−3131	54,606	17:39:24.304(6)	−31:31:15.3(6)	1.8887532968(2)	−66.311(2)	24.8(6)
J1740+1311	54,602	17:40:07.3455(11)	+13:11:56.69(2)	1.2452508156378(22)	−2.23747(2)	0.278(6)
J1741−3016	54,606	17:41:07.04(6)	−30:16:31(10)	0.5280523690760(10)	−2.51391(2)	-

Table 1. *Cont.*

PSR Name	Epoch	RAJ (h:m:s)	DECJ (d:m:s)	ν (Hz)	$\dot{\nu}$ ($\times 10^{-15}$ s^{-2})	$\ddot{\nu}$ ($\times 10^{-25}$ s^{-2})
J1744−3130	53,355	17:44:05.682(14)	−31:30:04(3)	0.938028884711(5)	−18.6732(3)	-
J1749−3002	55,633	17:49:13.49(3)	−30:02:35(4)	1.6396740787138(14)	−21.1858(3)	−0.25(17)
J1750−3157	54,595	17:50:47.318(9)	−31:57:44.1(6)	1.098462834370(1)	−0.23689(2)	-
J1756−2435	54,602	17:56:57.913(5)	−24:35:34(4)	1.491468585665(5)	−0.63314(4)	−0.036(11)
J1759−2205	54,603	17:59:24.149(3)	−22:05:32.8(19)	2.169297518784(8)	−51.15415(6)	2.88(2)
J1801−0357	54,626	18:01:22.647(4)	−03:57:55.19(18)	1.0851965795216(18)	−3.89516(2)	0.038(5)
J1805+0306	54,602	18:05:10.154(2)	+03:06:30.27(11)	4.572223444123(3)	−20.87328(3)	−0.024(9)
J1808−0813	54,606	18:08:09.432(10)	−08:13:01.80000	1.141494262394(3)	−1.613121(2)	0.105(7)
J1809−2109	54,544	18:09:14.329(4)	−21:09:02.90(14)	1.423659256988(4)	−7.74796(4)	0.060(12)
J1812−2102	54,591	18:12:20.95(2)	−21:02:41(6)	0.817421230445(6)	−15.97365(7)	0.040(2)
J1816−1729	54,551	18:16:18.662(5)	−17:29:02.7(7)	1.278254921960(4)	−11.95898(5)	−2.837(13)
J1820−1818	54,607	18:20:39.084(3)	−18:18:03.3(5)	3.2267991275985(15)	−0.97396(3)	-
J1823+0550	54,595	18:23:30.9724(19)	+05:50:24.29(6)	1.3281858693296(7)	−0.400066(14)	-
J1825−1446	54,550	18:25:02.939(6)	−14:46:53.0(6)	3.5817027826488(12)	−290.85139(7)	−1.77(24)
J1830−1059	54,593	18:30:47.566(10)	−10:59:27.9(5)	2.46871459375(8)	−365.3824(8)	15.5(2)
J1832−1021	54,607	18:32:40.866(2)	−10:21:32.78(14)	3.027037851445(14)	−38.45237(13)	1.61(4)
J1835−1020	54,324	18:35:57.5721(9)	−10:20:04.42(6)	3.306336424117(4)	−64.70088(5)	−0.970(14)
J1841−0345	54,595	18:41:38.688(12)	−03:48:43.0(5)	4.899970612570(4)	−1387.9497(10)	83.83(24)
J1841+0912	54,603	18:41:55.959(3)	+09:12:07.35(6)	2.622470024462(14)	−7.507076(13)	1.90(4)
J1844−0538	54,595	18:44:05.108(2)	−05:38:34.19(11)	3.91077944609(3)	−148.4690(3)	−0.04(8)
J1845−0743	54,618	18:45:57.1833(4)	−07:43:38.497(21)	9.5515883252959(23)	−33.45301(3)	−0.149(8)
J1849−0636	54,376	18:49:06.442(3)	−06:37:06.94(13)	0.68901746161314(18)	−21.952972(19)	0.010(7)
J1851+1259	54,594	18:51:13.215(7)	+12:59:35.29(15)	0.829663501119(13)	−7.825070(11)	0.04(3)
J1852−2610	54,608	18:52:59.467(13)	−26:10:12.7(18)	2.973206959232(5)	−0.77270(6)	0.037(16)
J1857+0212	54,560	18:57:43.642(3)	+02:12:41.11(11)	2.404768305012(3)	−232.81808(3)	2.849(10)
J1901+0331	54,546	19:01:31.781(2)	+03:31:05.97(7)	1.52566202812(4)	−17.3814(5)	−2.43(15)
J1901−0906	54,592	19:01:53.015(5)	−09:06:10.8(4)	0.5611898025495(6)	−0.515904(13)	-
J1904+0004	54,585	19:04:12.7180(15)	+00:04:05.29(4)	7.167191359472(8)	−6.06414(9)	−0.22(2)
J1906+0641	54,448	19:06:35.244(3)	+06:41:02.90(11)	3.741452121378(3)	−29.89305(3)	0.094(9)
J1910+0728	55,669	19:10:22.079(6)	+07:28:37.09(15)	3.072972409340(7)	−78.43730(14)	−0.68(9)
J1913+1400	54,238	19:13:24.3574(13)	+14:00:52.72(3)	1.9176447412047(25)	−2.95886(3)	0.03.1(11)
J1915+1647	53,575	19:15:19.10(3)	+16:47:08.5(6)	0.618723175122(15)	−0.1551(5)	-
J1916+1312	54,596	19:16:58.670(4)	+13:12:50.02(11)	3.5480620369(2)	−45.7486(17)	1.0(5)
J1919+0021	54,537	19:19:50.661(8)	+00:21:39.8(3)	0.7860005247324(13)	−4.74117(3)	-
J1922+2110	54,539	19:22:53.531(6)	+21:10:41.97(15)	0.927706045596(14)	−7.036766(14)	1.63(4)
J1926+1648	54,596	19:26:45.322(3)	+16:48:32.78(7)	1.724642861696(16)	−53.50760(13)	−0.70(4)
J1932+2220	54,546	19:32:22.74(3)	+22:20:51.5(5)	6.9211189179(6)	−2753.377(6)	121(2)
J1941−2602	54,590	19:41:00.416(3)	−26:02:05.77(24)	2.4822624468394(13)	−5.894042(11)	−0.053(4)
J1954+2923	54,606	19:54:22.531(3)	+29:23:16.67(5)	2.3436943701175(8)	−0.009347(8)	0.009(2)
J2002+3217	54,261	20:02:04.424(10)	+32:17:18.31(15)	1.43512309379(16)	−217.0140(16)	29.2(6)
J2023+5037	54,602	20:23:41.9545(13)	+50:37:35.144(13)	2.6836986452489(17)	−18.09913(2)	−0.385(5)
J2043+2740	55,660	20:43:43.5(1)	+27:40:56(1)	10.402450334(3)	−133.439(4)	−96(3)
J2055+3630	54,596	20:55:31.358(3)	+36:30:21.48(5)	4.514513533113(4)	−7.52119(4)	−0.098(12)
J2116+1414	54,539	21:16:13.756(7)	+14:14:20.74(14)	2.2719360939843(5)	−1.49470(6)	0.068(16)
J2150+5247	54,594	21:50:37.7331(19)	+52:47:49.625(18)	3.0101445811640(25)	−91.56954(2)	1.553(7)
J2225+6535	54,539	22:25:52.7677(3)	+65:35:35.865(1)	1.465110000716(7)	−20.72499(8)	0.82(2)
J2248−0101	54,595	22:48:26.904(18)	−01:01:48.1(7)	2.095411026501(6)	−2.89109(5)	−0.38(2)
J2308+5547	54,602	23:08:13.803(3)	+55:47:35.97(3)	2.1049627744054(13)	−0.884717(14)	0.052(4)
J2321+6024	54,133	23:21:55.197(3)	+60:24:30.74(6)	0.4431658815201(5)	−1.382686(3)	−0.0108(9)
J2330−2005	54,548	23:30:26.944(6)	−20:05:29.61(17)	0.6084116269097(11)	−1.714027(10)	−0.007(3)

* The uncertainties are given at the 1σ level in parentheses in the unit of the last quoted digit.

3.1. Rotational Parameters

The measured values of rotational parameters are consistent with those obtained in previous measurements except for PSR J1320−3512. With spin frequencies ranging from 0.3298 Hz to 10.4025 Hz, their spin frequency derivatives were determined to range from -3.11×10^{-18} s^{-2} to $-2753.377(6) \times 10^{-15}$ s^{-2}. The largest uncertainty in spin frequency is 6×10^{-10} Hz for the value of 6.9211189179 Hz at MJD 54,546 for PSR J1932+2220. The most precise measurement of spin frequency is achieved in PSR J1849−0636, with a ν of 0.68901746161314(18) Hz at MJD 54,376.

However, we detected a significant discrepancy in the spin-down rate of one pulsar. PSR J1320−3512 has a frequency derivative of $-3.10(3) \times 10^{-18}$ s^{-2}, as measured by the Nanshan radio telescope, which is inconsistent with the previously reported value of $-9(4) \times 10^{-18}$ s^{-2} [33]. This discrepancy in $\dot{\nu}$ is significant and may have originated from position inconsistency and timing noise, both of which affect the determination of spin parameters. Our new value indicates that the estimated characteristic age, $\tau_c = -\nu/(2\dot{\nu})$, for this pulsar increases from 3.82×10^9 yr to 1.11×10^{10} yr, making it the fifth oldest normal pulsar. The timing residuals are shown in Figures 1, A1 and A2.

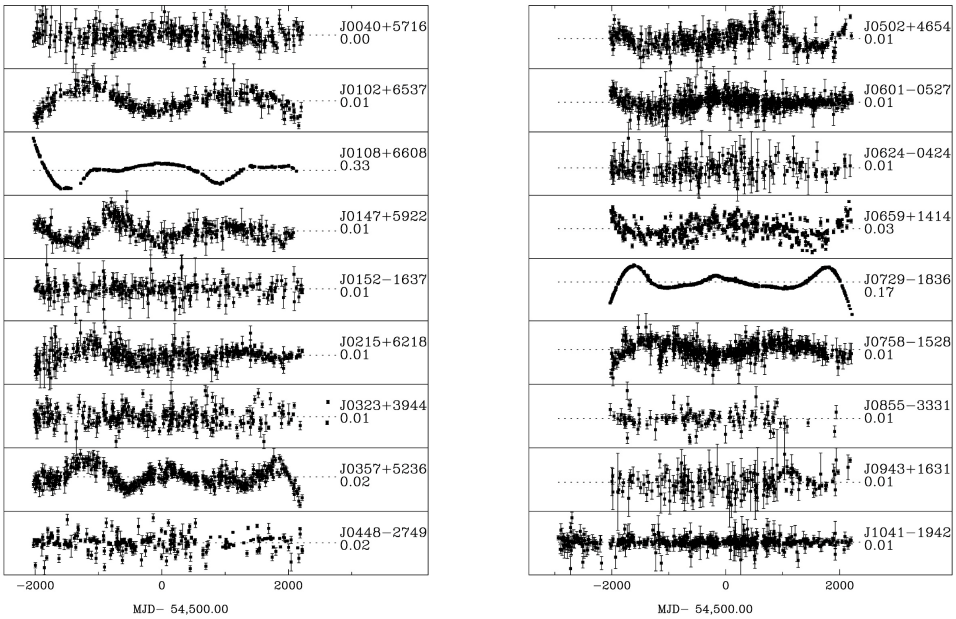

Figure 1. Timing residuals for 18 pulsars. The two labels on the right provide the pulsar name and phase range from the minimum to the maximum residuals. The timing residuals for other pulsars are plotted in Figures A1 and A2.

3.2. Power Spectra of The Timing Noise

The power density spectra for these pulsars are shown in Figure 2, displayed as a log–log plot of power spectral density against frequency. The spectral index (i.e., the logarithmic slope) was obtained by fitting the low-frequency spectra, where the spectral power exceeded the 1σ of the high-frequency white noise. For most of the spectra we obtained, white noise dominated at frequencies higher than 1.2 yr^{-1}. This implies that the shortest autocorrelation time detectable in the Nanshan pulsar observations is less than ~300 days. Moreover, it also indicates that the spectral turnover occurs around the frequency of 1.2 yr^{-1}, which is defined as the frequency at which the power law component reaches the white noise level [17]. The power spectra of timing noise with a spectral index (α) of -2, -4, and -6 theoretically corresponds to phase noise, frequency noise, and slow-down noise, respectively [16].

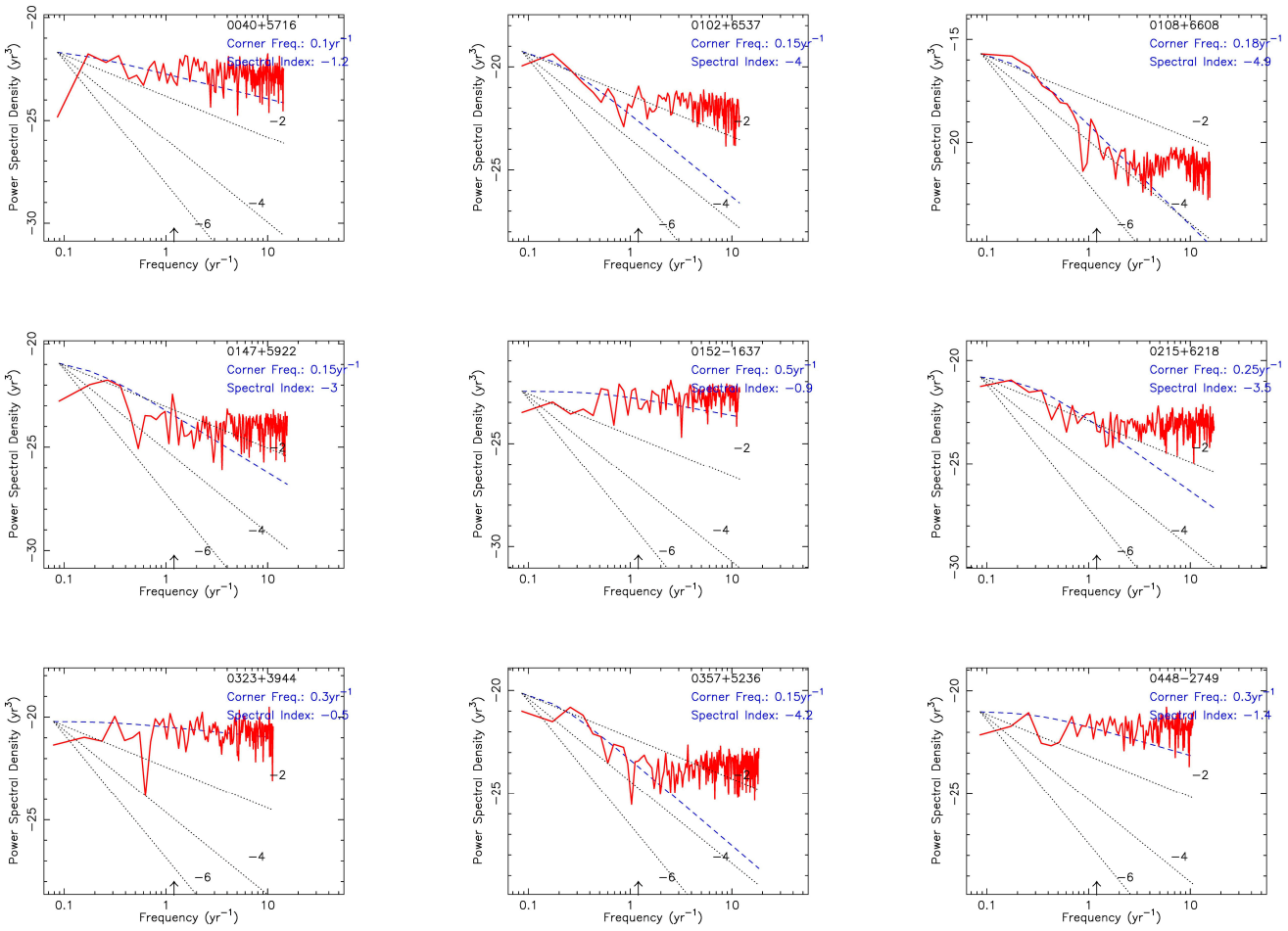

Figure 2. The power spectra of timing noise in nine pulsars. An arrow indicates the frequency of 1.2 yr^{-1}. A figure displaying power spectra for 85 pulsars is available online (see Supplementary Materials).

As depicted in Figure 1, no significant red noise is observed in 30 pulsars (e.g., J0040+5716, J0152−1637) with timing residuals exhibiting only white noise. These pulsars have spectral indices ranging from −2.2 to 0.1. Of these 30 pulsars, 16 (such as J0323+3944) present hardly any obvious $\ddot{\nu}$. The other 14 were detected with values of $\ddot{\nu}$ ranging from $-0.095(15) \times 10^{-25}$ s^{-3} to $0.105(7) \times 10^{-25}$ s^{-3}. For several pulsars, such as 1744−3130, J1852–2610, and J1901−0906, red noise is not noticeable at low frequencies, where the power spectra of these pulsars' timing noise are almost flat.

The spectra of PSRs J1741−3016, J1805+0306, and J1823+0550 have slopes of ∼−2, completely consistent with a phase noise process [17]. The timing noises in several pulsars, such as J0943+1631, J1711−1509, J1750−3157, and 1809−2109, show power spectra with spectral index between −1.8 and −2.2, suggesting that phase noise is predominant. The spectra of PSRs J0102+6537, J0502+4654, J1816−1729, J1926+1648, and J2225+6535 have slopes of ∼−4, fully consistent with an FN process [17]. PSRs J0357+5236, J0758−1528, and 2055+3630 exhibit spectra of timing noise with α values between −3.8 and −4, implying that spin frequency fluctuations dominate the timing noise. In relation to PSR J1749−3002, the timing noise spectrum has a spectral index of −6, indicating a spin-down noise process [17].

The timing noise in PSRs J0147+5922, J0215+6218, J0601−0527, J0659+1414, and others shows spectra with slopes in the range of −2.2 to −3.8, suggesting that these pulsars likely undergo a composite process involving phase noise and spin noise. The spectra of PSRs J0729−1836 and J1851 + 1259 have slopes of ∼−5.8−−6.2, suggesting a process dominated by spin-down noise.

Regarding 20 pulsars (PSRs J0108+6608, J1543+0929, J1722−3712, J1733−3716, J1739−3131, J1759−2205, J1825−1446, J1830−1059, J1832−1021, J1841−0345, J1841+0912,

J1844−0538, J1845−0743, J1857+0212, J1916+1312, J1922+2110, J1932+2220, J2002+3217, J2023+5037, and J2043+2740), their timing noise exhibits spectra with α values between −4.2 and −5.8, suggesting a composite process of spin noise and spin-down noise. The timing noise spectra in PSR J1901+0331 shows a very steep slope, with an index of −7. In addition to the random walk in the spin-down rate, the power spectrum of timing noise in J1932+2220 is unusual, as it seems that the white noise is only noticeable at higher frequencies (>10 yr^{-1}).

4. Discussion

The parameters of 85 pulsars and the noise models for stochastic noise processes are fitted to enable unbiased estimation of the ephemeris and to characterize the timing noise. It was shown that red noise is evident in normal pulsars. The timing behaviors of nine pulsars in our sample are consistent with random walks in the pulse phase, angular velocity, and torque. The timing noise spectra in 44 out of 85 (~52% of) pulsars have a spectral index between −7 and −3. The results imply that the primary sources of timing noise in our sample are likely from spin frequency irregularities, spin frequency derivative irregularities, or a composite process of spin noise and spin-down noise. However, the exact mechanism behind pulsar red noise is not fully understood. The causes of timing noise are proposed to include a fluctuating torque from the superfluid turbulence in the interior of a neutron star or structural inhomogeneity in the crust [34–36], the crustal seismic activity [37], magnetospheric state switching [38], long-term decay of magnetic fields [39], and evolution of magnetic inclination angle [40].

The flattened or white regions in the power spectra shown in Figure 2 can be explained by the presence of radiometer noise, pulse jitter, and internal superfluid components [17,41]. Some of the spectra, such as PSR J0357+5236 in Figure 2, resemble the low-frequency (frequency < 4.5×10^{-6} rad s^{-1}) power spectral density (PSD) for the angular velocity shown in Figure 6 of Antonelli et al. (2023) [17], implying that the timing noise in these pulsars originates from a random walk in spin frequency, leading to internal torque. Most of the pulsars reported in the article exhibit timing noise that is not well modeled by a random process with spectral indices of −2, −4, −6. Figure 3 illustrates the correlation between period derivative ($\dot{P}$) and spectral index, as reported in previous studies and this study [42–45]. It suggests that pulsars with higher $\dot{P}$ commonly have steep spectra of timing noise. This agrees with previous results, indicating pulsar timing activity is related to the loss of rotational energy. The gamma-ray pulsars were reported to have spectral indices α ranging from −9 to −5 [46], while this study obtained spectral indices (α) spanning from −7 to −1.

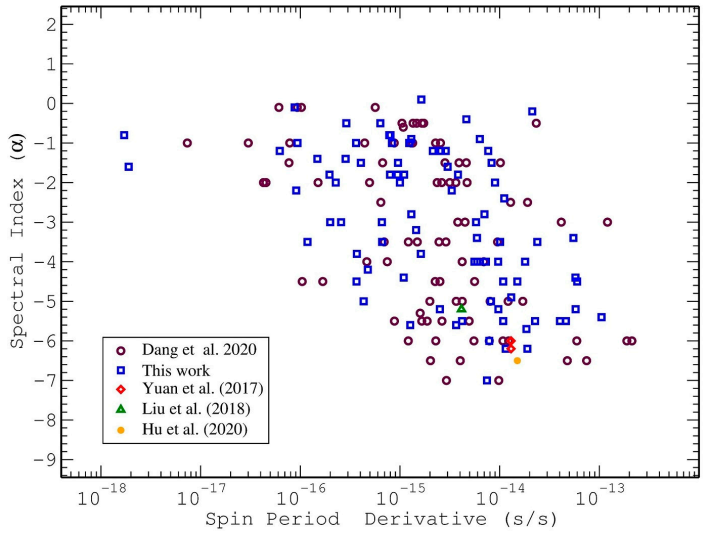

Figure 3. The correlation between spectral index and period derivative. The spectral index are obtained in previous studies [42–45] and this work.

However, the observed timing activity of certain pulsars may not reveal rotational irregularities, but rather changes in pulse profile and variations in dispersion measure (DM) [47]. DM variation will result in arrival time deviations of a microsecond or more for high DMs [48]. It has shown that solar wind leads to residual timing delays with a root-mean-square of microseconds [49]. Although the covariance between DM noise and rotational irregularities is included in our analysis, the DM noise is difficult to determine with the Nanshan radio telescope due to its sensitivity. An additional type of rotational irregularity, known as "slow glitch", has been identified in several radio pulsars [50], including PSR J1602−5100 [51]. Nevertheless, there is a claim that the slow glitch is a manifestation of timing noise [2].

5. Conclusions

We conducted timing analysis of 85 normal pulsars over a decade of observations using the Nanshan radio telescope, Xinjiang Astronomical Observatory. The positions and rotational parameters have been updated. A notable discrepancy in the spin-down rate has been detected for PSR J1320−3512 compared to previous observations. The timing behaviors of nine pulsars in our sample are consistent with random walks in the pulse phase, angular velocity, and torque. The timing noise spectra in 44 out of 85 (~52% of) pulsars have spectral index between −7 and −3. The results suggest that rotational irregularities are likely the primary sources of timing noise in half of our samples.

Supplementary Materials: The following supporting information can be downloaded at: https://www.mdpi.com/article/10.3390/universe10030105/s1, Figure S1: The power spectra of the timing noise in 85 pulsars.

Author Contributions: Conceptualization, N.W.; methodology, J.W.; software, Z.L. and R.Y.; validation, N.W. and L.L.; formal analysis, J.Y., S.D., F.K., Z.Z., P.L., and D.H.; investigation, J.Y.; resources, Z.W.; data curation, S.D.; writing—original draft preparation, J.Y.; writing—review and editing, S.D. and N.W.; visualization, J.W.; supervision, N.W.; project administration, N.W.; funding acquisition, W.Y. All authors have read and agreed to the published version of the manuscript.

Funding: This research was funded by the National Natural Science Foundation of China (grant numbers 12288102, 12041304, 12203093), the Major Science and Technology Program of Xinjiang Uygur Autonomous Region (No. 2022A03013-3, 2022A03013-4). S.D. is supported by Guizhou Provincial Science and Technology Foundation (No. ZK[2022]304) and the Scientific Research Project of the Guizhou Provincial Education (No. KY[2022]132). W.Y. is supported by the West Light Foundation of Chinese Academy of Sciences (No. WLFC 2021-XBQNXZ-027), the National Natural Science Foundation of China (NSFC) projects (No. 12273100, 12041303, 12288102), the National Key Program for Science and Technology Research and Development and the National SKA Program of China (No. 2022YFC2205201, 2020SKA0120200), the Natural Science Foundation of Xinjiang Uygur Autonomous Region (No. 2022D01D85), and the open program of the Key Laboratory of Xinjiang Uygur Autonomous Region (No. 2020D04049). Z.Z. acknowledges support from the Natural Science Basic Research Program of Shaanxi (Program No. 2024JC-YBQN-0036).

Data Availability Statement: The data that support the findings of this study are available from the corresponding author upon reasonable request.

Acknowledgments: The Nanshan Radio Telescope is operated by Xinjiang Astronomical Observatory and the Key Laboratory of Radio Astronomy, Chinese Academy of Sciences.

Conflicts of Interest: The authors declare no conflicts of interest. The funders had no role in the design of the study; in the collection, analyses, or interpretation of data; in the writing of the manuscript; or in the decision to publish the results.

Appendix A

The timing residuals of 67 pulsars are shown in Figures A1 and A2.

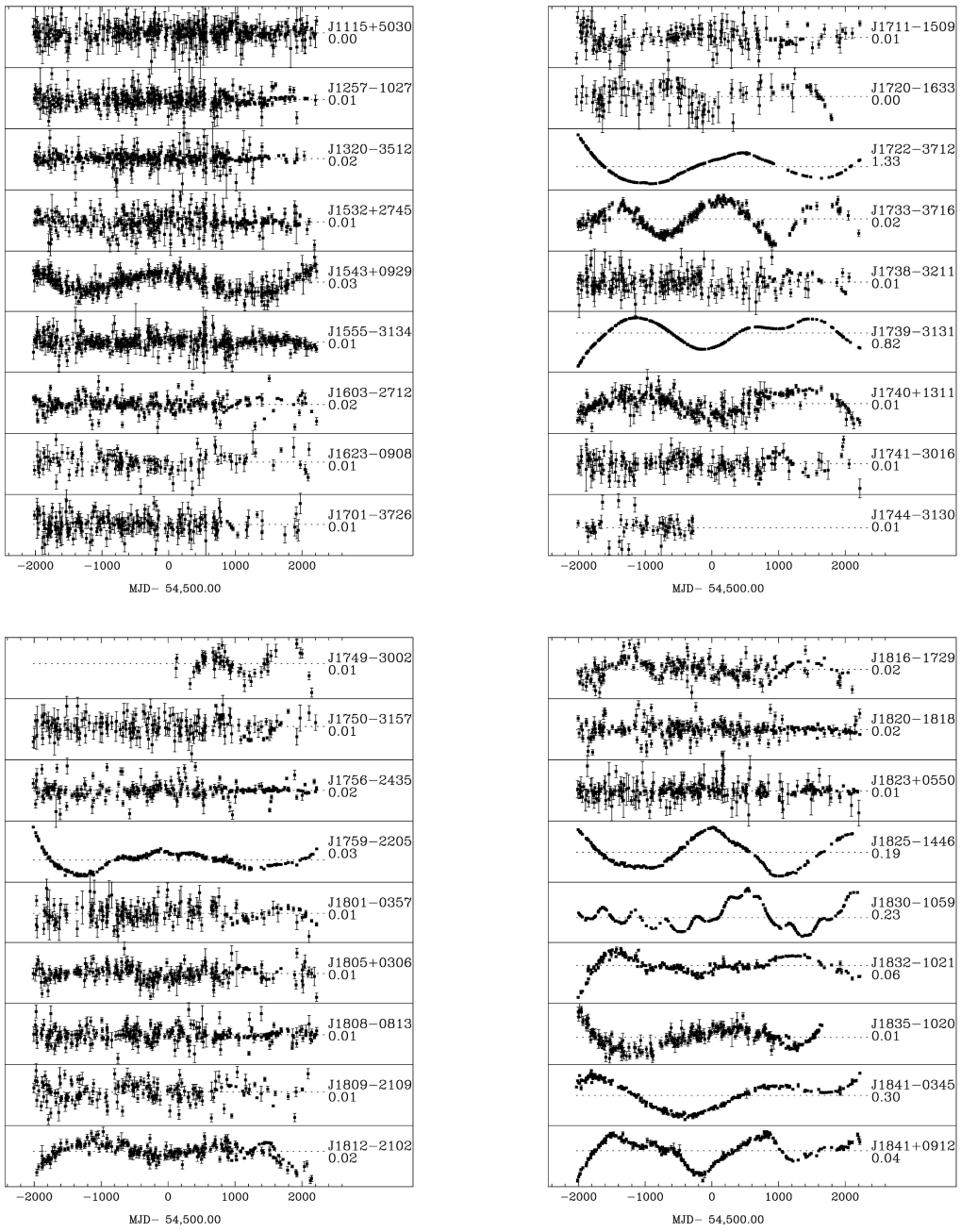

Figure A1. Timing residuals of 36 pulsars.

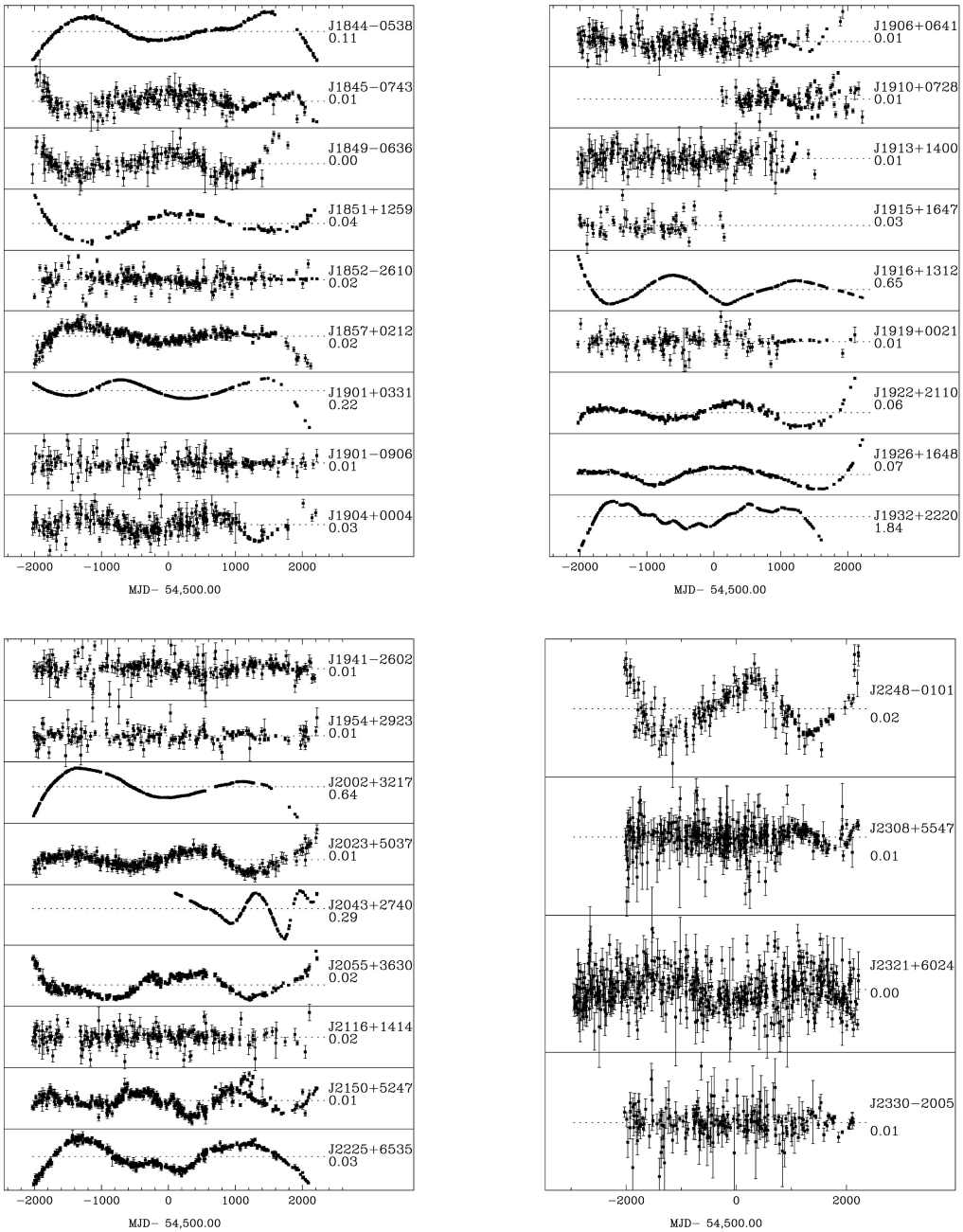

Figure A2. Timing residuals of 31 pulsars.

References

1. Haskell, B.; Melatos, A. Models of pulsar glitches. *Int. J. Mod. Phys. D* **2015**, *24*, 30008. [CrossRef]
2. Hobbs, G.; Lyne, A.G.; Kramer, M. An analysis of the timing irregularities for 366 pulsars. *Mon. Not. R. Astron. Soc.* **2010**, *402*, 1027–1048. [CrossRef]
3. Antonelli, M.; Montoli, A.; Pizzochero, P. *Insights into the Physics of Neutron Star Interiors from Pulsar Glitches, Astrophysics in the XXI Century with Compact Stars*; World Scientific: Singapore, 2022; p. 219.
4. Boynton, P.E.; Groth, E.J.; Hutchinson, D.P.; Nanos, G.P.; Partridge, R.B.; Wilkinson, D.T. Optical timing of the Crab pulsar, NP0532. *Astrophys. J.* **1972**, *175*, 217. [CrossRef]
5. Groth, E.J. Timing of the Crab pulsar. I. arrival times. *Astrophys. J. Ser.* **1975**, *29*, 431. [CrossRef]
6. Groth, E.J. Timing of the Crab pulsar II. Method of analysis. *Astrophys. J. Ser.* **1975**, *29*, 443–451. [CrossRef]
7. Cordes, J.M. Pulsar timing. II—Analysis of random walk timing noise—Application to the Crab pulsar. *Astrophys. J.* **1980**, *237*, 216. [CrossRef]
8. Cordes, J.M.; Downs, G.S. JPL pulsar timing observations. III—Pulsar rotation fluctuations. *Astrophys. J. Ser.* **1985**, *59*, 343. [CrossRef]

9. Cordes, J.M.; Downs, G.S.; Krause-Polstorff, J. JPL pulsar timing observations. V. macro- and Microjumps in the Vela pulsar. *Astrophys. J.* **1988**, *330*, 847. [CrossRef]
10. Arzoumanian, Z.; Nice, D.J.; Taylor, J.H.; Thorsett, S.E. Timing behavior of 96 radio pulsars. *Astrophys. J.* **1994**, *422*, 671. [CrossRef]
11. Parthasarathy, A.; Shannon, R.M.; Johnston, S.; Lentati, L.; Bailes, M.; Dai, S.; Kerr, M.; Manchester, R.N.; Osłowski, S.; Sobey, C.; et al. Timing of young radio pulsars—I. Timing noise, periodic modulation, and proper motion. *Mon. Not. R. Astron. Soc.* **2019**, *489*, 3810. [CrossRef]
12. Matsakis, D.N.; Taylor, J.H.; Eubanks, T.M. A statistic for describing pulsar and clock stabilities. *Astron. Astrophys.* **1997**, *326*, 924.
13. Lentati, L.; Alexander, P.; Hobson, M.P.; Taylor, S.; Gair, J.; Balan, S.T.; van Haasteren, R. Hyper-efficient model-independent Bayesian method for the analysis of pulsar timing data. *Phys. Rev. D* **2013**, *87*, 4021. [CrossRef]
14. Lower, M.E.; Johnston, S.; Dunn, L.; Shannon, R.M.; Bailes, M.; Dai, S.; Kerr, M.; Manchester, R.N.; Melatos, A.; Oswald, L.S.; et al. The impact of glitches on young pulsar rotational evolution. *Mon. Not. R. Astron. Soc.* **2021**, *508*, 3251. [CrossRef]
15. Ellis, J.A.; Vallisneri, M.; Taylor, S.R.; Baker, P.T. ENTERPRISE: Enhanced Numerical Toolbox Enabling a Robust PulsaR Inference SuitE. Available online: https://github.com/nanograv/enterprise (accessed on 22 February 2024).
16. Johnson, A.D.; Meyers, P.M.; Baker, P.T.; Cornish, N.J.; Hazboun, J.S.; Littenberg, T.B.; Romano, J.D.; Taylor, S.R.; Vallisneri, M.; Vigeland, S.J.; et al. The NANOGrav 15-year Gravitational-Wave Background Analysis Pipeline. *arXiv* **2023**, arXiv:2306.16223.
17. Antonelli, M.; Basu, A.; Haskell, B. Stochastic processes for pulsar timing noise: Fluctuations in the internal and external torques. *Mon. Not. R. Astron. Soc.* **2023**, *520*, 2813. [CrossRef]
18. Cordes, J.M.; Helfand, D.J. Pulsar timing III. timing noise of 50 pulsars. *Astrophys. J.* **1980**, *239*, 640. [CrossRef]
19. Deeter, J.E.; Boynton, P.E. Techniques for the estimation of red power spectra. I—Context and methodology. *Astrophys. J.* **1982**, *261*, 337. [CrossRef]
20. Deeter, J. Techniques for the estimation of red power spectra. II evaluation of alternative methods. *Astrophys. J.* **1984**, *281*, 482. [CrossRef]
21. Baykal, A.; Ali Alpar, M.; Boynton, P.E.; Deeter, J.E. The timing noise of PSR 0826+26, 1706−16, 1749−28, 2021+51 and the anomalous braking indices. *Mon. Not. R. Astron. Soc.* **1999**, *306*, 207. [CrossRef]
22. Deshpande, A.A.; D'Alessandro, F.; McCulloch, P.M. Application of 'CLEAN' in the power spectral analysis of non-uniformly sampled pulsar timing data. *J. Astrophys. Astron.* **1996**, *17*, 7. [CrossRef]
23. D'Alessandro, F.; Deshpande, A.A.; McCulloch, P.M. Power spectrum analysis of the timing noise in 18 southern pulsars. *JAstrophys. J.* **1997**, *18*, 5. [CrossRef]
24. Coles, W.; Hobbs, G.; Champion, D.J.; Manchester, R.N.; Verbiest, J.P.W. Pulsar timing analysis in the presence of correlated noise. *Mon. Not. R. Astron. Soc.* **2011**, *418*, 561. [CrossRef]
25. Wang, N.; Manchester, R.N.; Zhang, J.; Wu, X.J.; Yusup, A.; Lyne, A.G.; Cheng, K.S.; Chen, M.Z. Pulsar timing at Urumqi Astronomical Observatory: Observing system and results. *Mon. Not. R. Astron. Soc.* **2001**, *328*, 855. [CrossRef]
26. Zou, W.Z.; Wang, N.; Wang, H.X.; Manchester, R.N.; Wu, X.J.; Zhang, J. Unusual glitch behaviours of two young pulsars. *Mon. Not. R. Astron. Soc.* **2004**, *354*, 811. [CrossRef]
27. Manchester, R.N.; Hobbs, G.B.; Teoh, A.; Hobbs, M. The Australia Telescope National Facility Pulsar Catalogue. *Astrophys. J.* **2005**, *129*, 1993. [CrossRef]
28. Hotan, A.W.; van Straten, W.; Manchester, R.N. PSRCHIVE and PSRFITS: An open approach to radio pulsar data storage and analysis. *Publ. Astron. Soc. Aust.* **2004**, *21*, 302. [CrossRef]
29. Hobbs, G.B.; Edwards, R.T.; Manchester, R.N. TEMPO2, a new pulsar-timing package—I. An overview. *Mon. Not. R. Astron. Soc.* **2006**, *369*, 655. [CrossRef]
30. Edwards, R.T.; Hobbs, G.B.; Manchester, R.N. TEMPO2, a new pulsar-timing package—II. The timing model and precision estimates. *Mon. Not. R. Astron. Soc.* **2006**, *372*, 1549. [CrossRef]
31. Standish, E.M. Time scales in the JPL and CfA ephemerides. *Astron. Astrophys.* **1998**, *336*, 381.
32. Zhou, Z.R.; Wang, J.B.; Wang, N.; Yuan, J.P.; Kou, F.F.; Dang, S.J. Detection of 16 Small Glitches in Nine Pulsars. *Res. Astron. Astrophys.* **2022**, *22*, 5008. [CrossRef]
33. D'Amico, N.; Stappers, B.W.; Bailes, M.; Martin, C.E.; Bell, J.F.; Lyne, A.G.; Manchester, R.N. The Parkes southern pulsar survey—III. Timing of long-period pulsars. *Mon. Not. R. Astron. Soc.* **1998**, *297*, 28. [CrossRef]
34. Melatos, A.; Link, B. Pulsar timing noise from superfluid turbulence. *Mon. Not. R. Astron. Soc.* **2014**, *437*, 21. [CrossRef]
35. Cheng, K.S. Outer magnetospheric fluctuations and pulsar timing noise. *Astrophys. J.* **1987**, *321*, 799. [CrossRef]
36. Cheng, K.S. Could Glitches inducing magnetospheric fluctuations produce low-frequency pulsar timing noise? *Astrophys. J.* **1987**, *321*, 805. [CrossRef]
37. Kondratyev, V.N. Magnetoemission of Magnetars. *Phys. Part. Nucl.* **2019**, *50*, 613. [CrossRef]
38. Lyne, A.; Hobbs, G.; Kramer, M.; Stairs, I.; Stappers, B. Switched magnetospheric regulation of pulsar spin-down. *Science* **2010**, *329*, 408. [CrossRef] [PubMed]
39. Zhang, S.N.; Xie, Y. Test model of magnetic field evolution of neutron star with the statistical properties of their spin evolution. *Astrophys. J.* **2012**, *757*, 153. [CrossRef]
40. Yi, S.-X.; Zhang, S.-N. The evolution of the magnetic inclination angle as an explanation of the long term red timing-noise of pulsars. *Mon. Not. R. Astron. Soc.* **2015**, *454*, 3674. [CrossRef]

41. Parthasarathy, A.; Bailes, M.; Shannon, R.M.; van Straten, W.; Osłowski, S.; Johnston, S.; Spiewak, R.; Reardon, D.J.; Kramer, M.; Venkatraman Krishnan, V.; et al. Measurements of pulse jitter and single-pulse variability in millisecond pulsars using MeerKAT. *Mon. Not. R. Astron. Soc.* **2021**, *502*, 407. [CrossRef]
42. Yuan, J.P.; Manchester, R.N.; Wang, N.; Wang, J.B.; Zhou, X.; Yan, W.M.; Liu, Z.Y. Pulse profiles and timing of PSR J1757-2421. *Mon. Not. R. Astron. Soc.* **2017**, *466*, 1234. [CrossRef]
43. Liu, Y.L.; Yuan, J.P.; Wang, J.B.; Liu, X.W.; Wang, N.; Yuen, R. Timing irregularities of PSR J1705-1906. *Astrophys. Space Sci.* **2018**, *363*, 96. [CrossRef]
44. Dang, S.J.; Yuan, J.P.; Manchester, R.N.; Li, L.; Wang, N.; Wang, J.B.; Hobbs, G.; Kou, F.F. Results of 12 yr of pulsar timing at Nanshan. I. *Astrophys. J.* **2020**, *896*, 140. [CrossRef]
45. Hu, Y.; Li, L.; Yuan, J.P.; Dang, S.J.; Wang, S.Q.; Wang, Z.J.; Yuen, R. Timing and emission variation of PSR J1733-3716. *Astrophys. Space Sci.* **2020**, *365*, 143.
46. Kerr, M.; Ray, P.S.; Johnston, S.; Shannon, R.M.; Camilo, F. Timing Gamma-ray Pulsars with the Fermi Large Area Telescope: Timing Noise and Astrometry. *Astrophys. J.* **2015**, *814*, 128. [CrossRef]
47. Keith, M.J.; Coles, W.; Shannon, R.M.; Hobbs, G.B.; Manchester, R.N.; Bailes, M.; Bhat, N.D.R.; Burke-Spolaor, S.; Champion, D.J.; Chaudhary, A.; et al. Measurement and correction of variations in interstellar dispersion in high-precision pulsar timing. *Mon. Not. R. Astron. Soc.* **2013**, *429*, 2161. [CrossRef]
48. Cordes, J.M.; Shannon, R.M.; Stinebring, D.R. Frequency-dependent Dispersion Measures and Implications for Pulsar Timing. *Astrophys. J.* **2016**, *817*, 16. [CrossRef]
49. Tiburzi, C.; Shaifullah, G.M.; Bassa, C.G.; Zucca, P.; Verbiest, J.P.W.; Porayko, N.K.; van der Wateren, E.; Fallows, R.A.; Main, R.A.; Janssen, G.H.; et al. The impact of solar wind variability on pulsar timing. *Astron. Astrophys.* **2021**, *647*, 84. [CrossRef]
50. Greenstein, G. Pulsar Glitches, Fast and Slow. *Bull. Am. Astron. Soc.* **1979**, *11*, 426.
51. Zhou, S.; Gügercinoğlu, E.; Yuan, J.; Ge, M.; Yu, C. Pulsar Glitches: A Review. *Universe* **2022**, *8*, 641. [CrossRef]